JrnlID 11340_ArtID 9926_Proof# 1 - 02/07/2014

Experimental Mechanics
DOI 10.1007/s11340-014-9926-7

# Experimental Methodology for Studying Strain Heterogeneity with Microstructural Data from High Temperature Deformation

**Garrett J. Pataky · Huseyin Sehitoglu**

Received: 4 November 2013 / Accepted: 27 June 2014


**Abstract** An experimental methodology has been developed to study materials deformed at high temperatures using high resolution *ex situ* digital image correlation (DIC). This study is an advancement of techniques that have used sub-grain level strain measurements and linked them to microstructural data obtained with electron back-scatter diffraction (EBSD). The approach utilized air blasting particles that were capable of remaining unchanged onto a sample surface and loading the sample at elevated temperatures in vacuum to prevent oxidation. Two tensile experiments were performed at temperatures of 700 and 800 °C on Haynes 230 (a nickel-based superalloy) using DIC at high magnifications in order to study the heterogeneous strain fields. Overlaying the strain fields and microstructure data, areas of high strain were studied at a grain boundary, triple junction of boundaries, and at a slip band. The strain evolution at these areas was compared to the mean strain accumulation. This study represents an advancement of the usefulness of high resolution DIC by expanding the loading conditions that can be studied and provided experimental results to prove the feasibility.

**Keywords** Digital image correlation · Electron backscattering · Microstructure · High temperature · Experimental procedure · Deformation

G.J. Pataky (✉) · H. Sehitoglu
Department of Mechanical Science and Engineering, University of Illinois at Urbana-Champaign, 1206 W. Green St., Urbana, IL 61801, USA
e-mail: pataky2@illinois.edu

H. Sehitoglu
e-mail: huseyin@illinois.edu

## Introduction

To assist the development of physically based models, there is a need to experimentally study strain heterogeneities at the sub-grain level [1–3]. There have been continual developments to increase the resolution of measurement techniques in order to meet this demand. Many studies have successfully linked strains to the microstructure using electron back-scatter diffraction (EBSD). Currently, there are few high resolution experimental studies performed on materials deformed at high temperatures [4, 5]. The present study will focus on describing the experimental methodology developed in order to study a nickel-based superalloy at high temperatures using sub-grain measurements from digital image correlation (DIC) along with preliminary results of two tensile tests.

Two experimental, optical methods have emerged as being useful for studying strain heterogeneities. The first method is a grid method used by several researchers [6–8]. An explanation of this displacement measurement technique can be found in [9]. The problem with this measurement technique is that localized high gradients have been found to be difficult to detect [6]. The current study aims to observe the strain heterogeneities across grain boundaries, twin boundaries, and carbides, and thus the ability to measure these high gradients is extremely important.

The second method to experimentally measure displacements is digital image correlation (DIC). Instead of tracking a grid during deformation, DIC uses the light intensity of each pixel in the full-field, separated into unique boxes called subsets, to quantitatively measure displacements. There is no inherent length scale for DIC and a higher resolution measurement is produced by increasing the magnification of the images captured. This allows for sub-grain level measurements without a large grain size. A more detailed description of the DIC technique is given in [10].

Two approaches to the experiments are possible. *In situ* provides measurements during loading without having to remove the specimen in order to capture images. This has been widely used by researchers to study, for example, fatigue crack growth [11, 12] and monotonic loading [13]. The issue with the *in-situ* approach is that it generally must be performed at lower magnifications in order to avoid being affected by vibrations causing blurring of the images. In order to circumvent this issue, special load frames have been used in conjunction with scanning electron microscopes (SEM) or optical microscopes [8, 14, 15]. There is a limitation to this though; it is difficult to produce high temperature experiments without damaging the equipment and specimen geometries are limited. The other approach, *ex situ*, is not limited by the experimental setup or environment, including high temperature, since the sample is removed from the testing apparatus before imaging. This method can be performed either optically or in the SEM. Optical microscopes are limited in their depth of focus, which is detrimental in the case of out of plane displacements. Using an SEM, higher magnifications can be achieved, but this is not without its own issues. Drift during image capture and background noise affecting the pattern are two of the major problems [16]. An optical microscope was used in this study in order to circumvent these drawbacks since out of plane displacements will be small.

The present study will introduce a high resolution DIC *ex situ* experimental methodology in for studying materials deformed at high temperatures. The strain fields of a predetermined area will be measured and related to the microstructure using data found from EBSD. The procedure used is an advancement of the one developed by Carroll et al. during a similar study performed on materials at room temperatures [17]. The results from Haynes 230, a nickel-based superalloy, deformed at 700 °C and 800 °C under monotonic loading will be shown using this technique. The abilities developed by this study will be a clear advancement for studying strain heterogeneity in materials in a high temperature environment.

## Experimental Procedure

The following section will outline the experimental procedure used to perform *ex situ* high resolution DIC. This methodology has been utilized to study a nickel-based superalloy at 700 °C and 800 °C. Every step of the experiment will be described including the sample preparation, experimental setup, deformation analysis, and alignment of the DIC strain fields to the microstructure data obtained using EBSD.

### Sample Preparation

In order to perform EBSD and get information about the microstructure, the samples must be polished to a mirror finish. The specimens used during this study were "dog-bone" shaped with a gauge length of 25.00 mm, width of 4.00 mm, and a thickness of 2.38 mm. This procedure is not limited by the specimen shape or size, thus any specimen can be used. The samples were mechanically polished with abrasive grinding paper up to a grit of P4000. The sample was then polished using 0.3 μm silica powder and finalized with a vibropolisher.

Before the microstructure was characterized, the area of interest on the sample surface needed to be marked. A discussion of the requirements for these marks is given by Carroll et al. with Vickers indentation marks being determined as ideal [17]. The main requirements of these markings were that they need to last throughout the entirety of the experiment so all data sets can be linked, and they must be small enough to align with the microstructure. Five Vickers marks were used to mark off a rectangular area of 1.05 mm by 0.525 mm. The fifth mark was made next to one of the corners to discern the alignment of the area. EBSD was performed in a JEOL 7,000 F SEM with measurement spacing of 1.0 μm. Due to the size of the area of interest, multiple EBSD scans were made. These were aligned and joined with the CHANNEL 5 software package. Figure 1 shows a schematic of the sample used, the location of the area of interest, and the EBSD scan of the area.

The next step of the experiment was to speckle the sample surface in order to use DIC. This was a major area of concern since anything on the surface can be destroyed by the elevated temperatures thus destroying the speckle pattern. There are a couple requirements that must be met. First, the speckles of the pattern must be small enough in order to produce sub-grain quality measurements. The material deposited on the surface must be able to withstand the temperature of the experiment as well. Depositing particles onto the surface using compressed air was identified as the best method, as first used by Jonnalagadda et al. [18]. This is due to the consistency a pattern can be made without worrying about having random large speckles, as seen with spraying paint, and the large range of materials available to deposit. Two types of particles were tested, 1 μm diameter Si and 0.3 μm alumina. Once deposited on the surface, both types of particles provided good DIC speckle patterns, Si shown in Fig. 2a and alumina shown in Fig. 2b. After heating to 800 °C in vacuum, cooling, and removing, it was immediately obvious that the Si would not suitable for this application (Fig. 2c) but the alumina remained unchanged (Fig. 2d). This example expounded the second requirement for the speckle material.

### Experimental Procedure

The procedure outlined is for performing 2-D DIC for a material deformed under high temperature conditions. A vacuum system is employed in order to prevent oxidation which would destroy the DIC speckle pattern. Since the

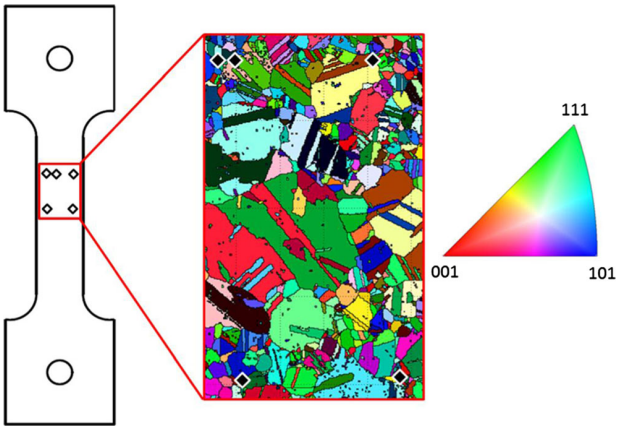


**Fig. 1** A schematic of the "dog-bone" specimen with the location of the area studied defined by the Vickers indentation marks. The EBSD scan results showing grain orientations with the Vickers marks accentuated

heterogeneity of the strain field at the microstructural level is desired, a microscope has been used to capture the images. This allows for higher spatial resolution compared to previous high temperature DIC studies [13, 19]. The following section outlines the equipment used and the procedure performed.

An initial set of images of the sample surface with the alumina speckle pattern (Section 2.1) was taken as the DIC reference images. Since the DIC measurement resolution is based on the imaging magnification, consideration must be made to choose a magnification that will elucidate the desired sub-grain level measurements. A limitation to using higher magnifications was the reduced area that each image captured. In order to circumvent this issue, multiple images must be taken in order to capture the entire area of interest. In this study, an optical microscope and two magnifications were used with an IMI 202FT digital camera that had a resolution of 1,600 pix by 1,200 pix. The lower magnification used was 10× which corresponded to a scale of 0.437 μm/pix and a higher magnification of 25× which corresponded to a scale of 0.175 μm/pix. 3 images at the magnification of 10× and 27 images at the magnification of 25× were required to cover the entire area of interest. The explanation on how to handle the image array will be covered in Section 2.3.

After the set of references images was taken, the sample was ready to be prepared for the experiment. A vacuum or inert environment is necessary to safeguard against uncontrollable pattern changes once the sample is taken to temperature during testing. A vacuum chamber was utilized during this study to protect the sample surface from oxidation. A picture showing the vacuum chamber and load frame used during this study is given in Fig. 3. The specimen had a type-K thermocouple spot welded onto the middle of the back once placed into the load frame. The chamber was then sealed and pulled into a vacuum of $10^{-6}$ Torr. Once this level was reached, which typically took pumping the system overnight, the sample was heated using induction heating at a rate of 75 °C per minute. Once the specimen had reached the desired temperature, 700 °C or 800 °C for this study, the temperature was kept to a tolerance of±3 °C for the duration of the deformation step using a temperature controller connected to the induction heater. The specimen was then loaded with a servo-hydraulic load frame. After the desired amount of deformation, monotonic tension at a strain rate of $10^{-4}$ $s^{-1}$ in this study, was reached, the system was cooled down to room temperature before returning the chamber to atmospheric pressure. This was to guarantee that there would be no avoidable surface

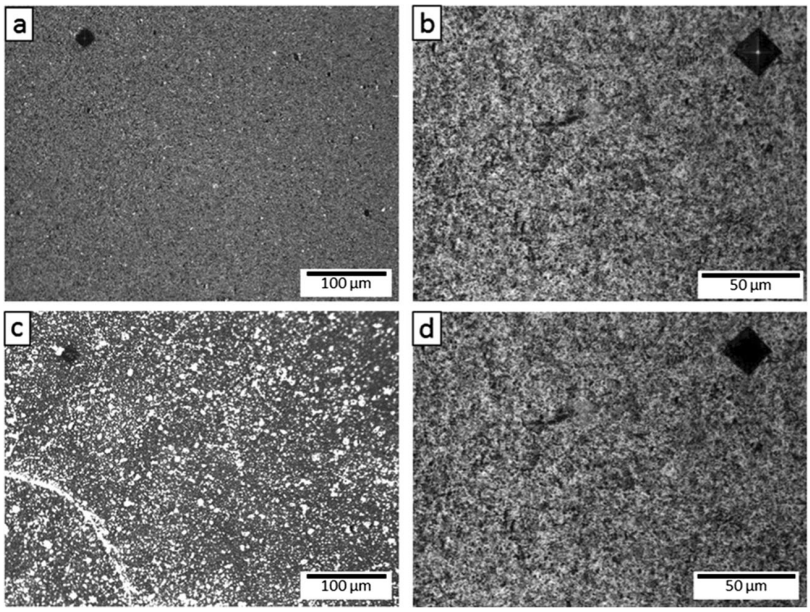


**Fig. 2** Speckle patterns of air blasted (**a**) Si particles (10× magnification) and (**b**) alumina particles (25× magnifications) before heating taken using the optical microscope. (**c**) The pattern with the Si particles changed drastically after being heated to 800 °C while the (**d**) alumina particle pattern remained consistent with the unheated pattern

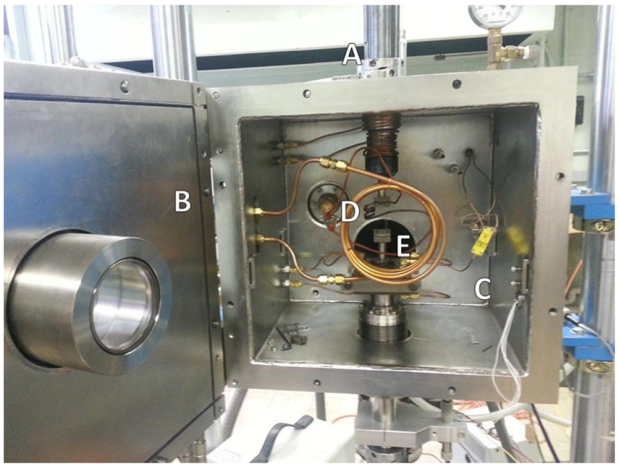


**Fig. 3** A picture of the experimental setup showing: (**a**) load frame, (**b**) vacuum chamber, (**c**) type-K thermocouple, (**d**) induction heating coils, and (**e**) grips where specimen was placed. The copper coiling is to provide cooling during the experiments at elevated temperatures

changes. The sample was then removed from the chamber and the thermocouple taken off. Images of the deformed surface were then captured with the optical microscope in the same method that the reference images were captured. The Vickers markers made visually identifying the area of interest easy. It is pertinent to capture the images in the same pattern as the reference images to avoid any unnecessary post-processing changes. Once the imaging was completed, the procedure of attaching the thermocouple, pulling vacuum, heating the sample, and then deforming was repeated. For the experiment performed at 800 °C two deformation steps were made and for the 700 °C experiment ten deformation steps were made.

## Analysis

After deformation and image capture, the next step was to analyze the data using DIC. Since this method is an *ex situ* technique, the strain fields found will be the residual plastic strains. There will be two methods discussed for completing this since multiple images were required to cover the area of interest: stitching the images and stitching the DIC results. Both methods were used during this study. The first technique, stitching the images and then correlating, was used for the images magnified at 25× in the 800 °C experiment and the images magnified at 10× in the 700 °C experiment. The stitching of the images was performed with a stitching plug-in available in the open-source, image processing package FIJI [20]. The plug-in uses a Fourier Shift Theorem that computes all possible translations in order to find the optimal overlapping. Each set of images, reference and deformed, was stitched yielding a fused image. The deformed images were then correlated to the reference images using commercial DIC software. There is a couple drawbacks to this technique. The 25× magnification stitched images were very large, over 100 megabytes, and this exceeded the limit of the software to correlate, and the stitching seams have been found to produce artificial strains [17]. It is important to note that both times the 25× magnification was utilized, the correlating parameters were kept the same.

The second method to handle the image array is to perform DIC on each individual image and then combine those results as developed by Carroll et al. [17]. This approach was used for each set of the 27 images taken at the 25× magnification during the 700 °C experiment. Each of these images was overlapping by 40–50 % to create enough overlapping data to match up the DIC results sufficiently. This produced 11 sets of 27 strain fields (the reference and 10 deformed sets). Deformation caused each of the strain fields to be at a slightly different location. To get a reference location for the strain fields, the reference images were stitched together using FIJI, as previously discussed, providing their original locations. Subsequently the strain fields were interpolated into an evenly spaced grid, mimicking a DIC subset grid, to produce the entire full-field strain field using these original locations. The strains were stitched to alleviate the issue of seams producing errors since this stitching occurred post-correlation. This reduced the error down to interpolation instead of artificial strains.

The final step was to align the DIC strain fields and the microstructure data from the EBSD. This was done using the Vickers marks made on the surface of the specimen at the start of the experiment. The Vickers marks are difficult to determine their exact location and size from the strain fields, so the first step was to overlay each of the strain fields onto the stitched reference image since these locations are known. This was possible with software that allows layers, such as Adobe Photoshop or the open-source software GIMP. Then the EBSD data can be overlaid onto the stitched reference image by aligning the Vickers marks. This required some manipulation to the EBSD data since it was skewed and rotated. After this was completed, the stitched reference image was removed leaving the strain fields and microstructural data aligned. It was then possible to determine how the grain boundaries, twin boundaries, and carbides affected the strain heterogeneity. Each of the boundary types are known as well so it is possible to do statistical analysis such as in references [21, 22].

## Results and Discussion

The following section will present the results from the monotonic tension experiments performed at 700 and 800 °C and analyzed using the high resolution *ex situ* DIC technique presented in this paper. The 800 °C experiment produced large scale cracking after two deformation steps. Subsequently, the

700 °C was performed and ten deformation steps were able to be produced.

## Measurement Error

When performing DIC, one of the major concerns is the amount of measurement error present. It was concluded in an earlier study that the image stitching technique provided a larger amount of error than the DIC stitching technique [17]. The following will cover the error determined for this study based on the $\varepsilon_{yy}$ strain since this was the component presented in this study.

The first step in reducing the error was to ensure that the specimen was inserted into the microscope in a consistent manner. A custom slide was designed in order to hold the specimen in the same spot and orientation each time it was placed on the microscope. The slide was designed so it could be attached to the microscope easily and was rigidly attached.

The error analysis is based on the 700 °C experiment since the out of plane displacements due to cracking were not observed. Two sets of reference images at 10× magnification for the 700 °C experiment were captured for the error analysis. This was done by taking one complete set of images, removing the specimen from the microscope, and then replacing the specimen and capturing the second set of images. The microscope settings (brightness, shutter speed, sharpness, etc.) were kept the same. This provided a base set of two reference, stitched images in which the average strains throughout the entire experiment could be compared. Each stitched deformation image was correlated to the same area of interest for both of the reference images. Table 1 gives the comparison between the mean $\varepsilon_{yy}$ strains found. The results showed a maximum background error of 0.0023 %. Although impressive, the local error is an important number to consider since this study concentrated on the strain heterogeneity. To find the local error, the entire field was analyzed for the highest strain difference between the two identical fields. The two reference images were correlated to each other, both being undeformed, and the maximum local error was found to be orders of magnitude higher at 0.11 %. The local error was determined again using the tenth deformation step by finding the maximum difference between correlations when correlating this image array to both of the undeformed, reference images. The magnitude of error measured was to be 0.20 %. It must be noted that this was determined at a region with strain over 2 %.

A similar error analysis was performed with the 25× magnification images. This procedure was performed with the DIC data stitching method. When comparing two undeformed sets of images, the mean $\varepsilon_{yy}$ strain error was found to be 0.0096 %. This was on the order found with the 10× magnification. The local error was found to have increased to 0.34 %. When taking into consideration the strains found at the areas of concentration studied in Section 3.3, the result is a low amount of error.

**Table 1** A comparison of the DIC mean $\varepsilon_{yy}$ strain values over the entire area of interest correlated to each of the two 10× magnification reference images

| | Reference 1 | Reference 2 | Difference |
|---|---|---|---|
| Step 1 | 0.022 % | 0.024 % | 0.0018 % |
| Step 2 | 0.295 % | 0.297 % | 0.0013 % |
| Step 3 | 1.061 % | 1.062 % | 0.0012 % |
| Step 4 | 1.216 % | 1.218 % | 0.0020 % |
| Step 5 | 1.369 % | 1.370 % | 0.0015 % |
| Step 6 | 1.586 % | 1.587 % | 0.0016 % |
| Step 7 | 1.872 % | 1.874 % | 0.0016 % |
| Step 8 | 1.961 % | 1.963 % | 0.0020 % |
| Step 9 | 2.511 % | 2.513 % | 0.0022 % |
| Step 10 | 3.094 % | 3.096 % | 0.0023 % |

## Material

The material used during this study was the nickel-based superalloy Haynes 230. Haynes 230 is a solid-solution strengthened alloy that was developed for high temperature applications and thus has additions of tungsten, chromium, and molybdenum. The grains were found to be equiaxed with grain sizes ranging from 30 μm to 250 μm. The EBSD data showed a large amount of annealing twins and two-thirds of the boundaries were observed to be ∑3 boundaries following the coincident lattice notation (CSL). An example of the microstructure was given in Fig. 1.

The results of tensile tests performed at room temperature, 700, and 800 °C are given in Fig. 4. All three experiments were run at a strain rate of $10^{-4}$ $s^{-1}$. The yield stress for each temperature was found using a 0.2 % offset. This value was found to be 415 MPa at room temperature, 302 MPa at 700 °C, and 197 MPa at 800 °C. Hardening was observed in the room temperature results and initially in the 700 °C results, while the 800 °C results showed softening. Serrations in the 700 °C stress–strain curve were attributed to the Portevin-Le Chatelier effect, but not in the 800 °C stress–strain curve. This has also been found in other similar nickel-based superalloys, such as Hastelloy X [23].

## 800 °C Tensile Test

Two steps of deformation were made at 800 °C using the experimental technique outlined in Section 2. A 51 pix by 51 pix (8.9 μm by 8.9 μm) subset size with a step of 5 pix (0.875 μm) was used for the DIC analysis. The first step was measured at a mean $\varepsilon_{yy}$ strain of 0.8 %, and the second at 5.5 %. During the second step, many cracks formed on the

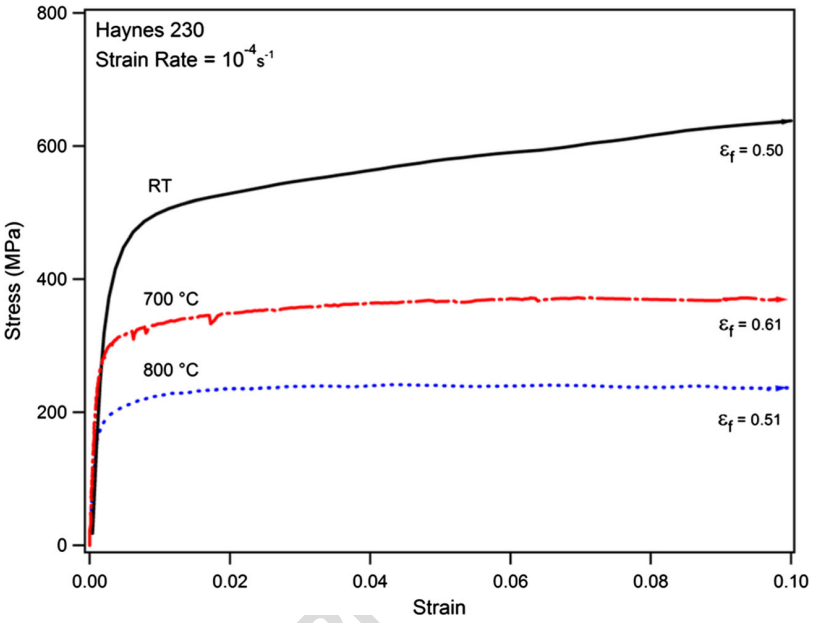


**Fig. 4** The stress–strain response of Haynes 230 at room temperature (RT), 700 °C, and 800 °C

Haynes 230 sample. These showed up as very high strains (over 15 %) in DIC and thus the 5.5 % of mean strain was considered to be an overestimation. The stitched reference image, stitched first step image, and the DIC results are given in Fig. 5a–c respectively. It is clear that even with the mean strain under 1 %, there was a heterogeneous strain field present. Areas with strains over 2.5 % occurred throughout.

Due to the crack formation on the Haynes 230 sample after the second deformation step, the sample surface rose in certain areas which made it impossible to capture the complete area of interest while still in focus. This phenomenon was not present in the entire area of interest and the change in focus followed the crack paths. An example of one section is given in Fig. 6. In Fig. 6a and b, the red dotted line depicts the divide between the focuses. There was a simple procedure to solve this dilemma. Capturing images at different focuses (Fig. 6a and b) and then combining them in software that allows layers, such as the earlier mentioned Adobe Photoshop or GIMP, provided

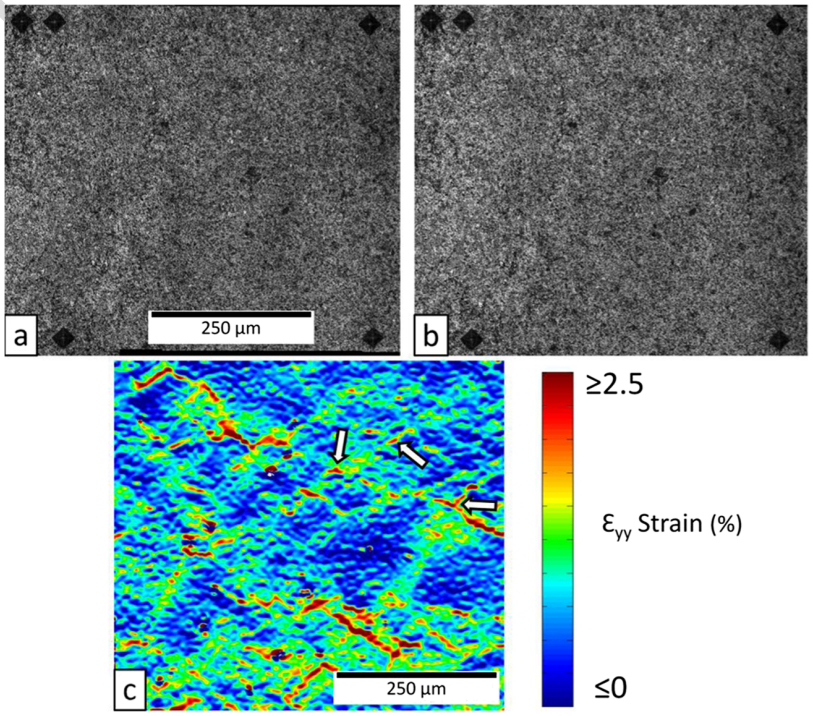


**Fig. 5** Images from the optical microscope showing the 0.6 mm by 0.6 mm area and speckle pattern of the sample tested at 800 °C (**a**) undeformed and (**b**) after the first step of heating and deformation at a magnification of 25× with the Vickers indentation marks visible. (**c**) The $\varepsilon_{yy}$ strain field found using DIC. The white arrows in (**c**) show high strained areas that crack in the next deformation step (shown in Fig. 6c)

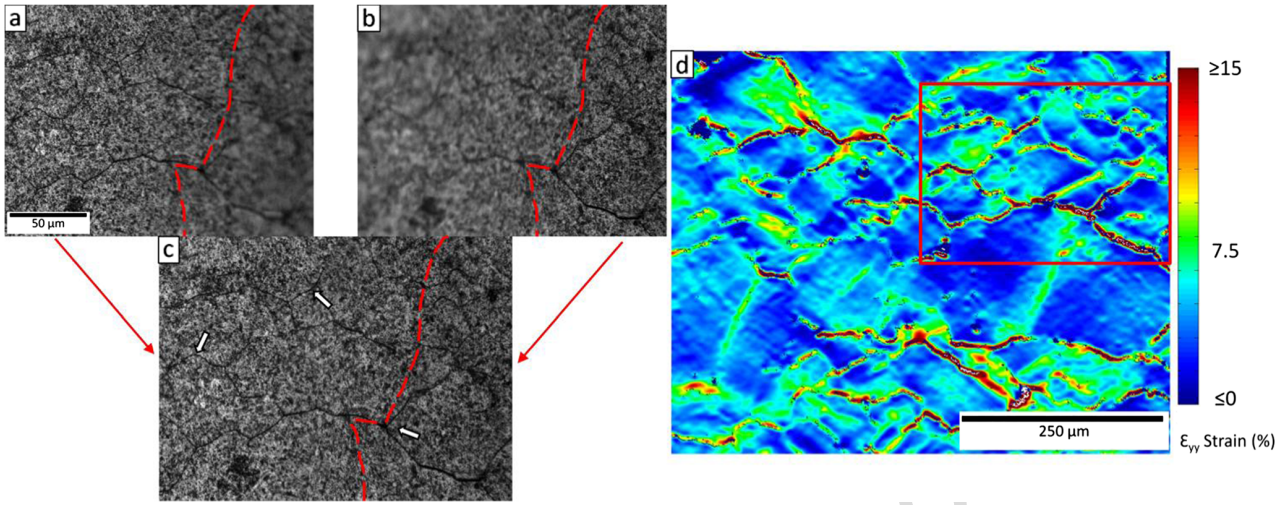


**Fig. 6** (**a**) and (**b**) Images taken with the optical microscope depicting the lack of focus in certain areas of each image. (**c**) The combined image created using the images in (**a**) and (**b**) and eliminating the out of focus regions. (**d**) The $\varepsilon_{yy}$ strain field found using DIC with cracks on the sample showing strain magnitudes of 15 % or greater. The red box is the region correlated using the image in (**c**). The white arrows in (**c**) show cracked regions that were the highly strained areas in the previous deformation step

the base. By eliminating the areas out of focus on the top layer, an image that has full focus is obtained, as shown in Fig. 6c. Once this was completed, the DIC correlation was performed and the axial strain results are given in Fig. 6d. The red box identifies the area from Fig. 6c, showing the success of this technique. It must be stated that since this is a manual manipulation technique, this procedure should be limited to prevent the introduction of error. Comparing Figs. 5c and 6c, there was a clear correlation between the areas of high strain concentration in the first step and the eventual crack locations in the second step. Three of the high strain regions which cracked are highlighted with white arrows. A majority of these cracks were along grain boundaries.

## 700 °C Tensile Test

This tensile experiment was performed at 700 °C and included 10 deformation steps. Two magnifications were used. The images taken at a magnification of 10× were analyzed using the image stitching technique, while the images taken at 25× magnification were analyzed using the DIC data stitching technique. The DIC analysis for the 10× magnification was performed with a 31 pix by 31 pix (13.55 μm by 13.55 μm) subset size with a step of 5 pix (2.185 μm) and the 25× magnification analysis was performed with the same subset as the 800 °C test, 51 pix by 51 pix (8.9 μm by 8.9 μm) subset size with a step size of 5 pix (0.875 μm). The reason for using the lower magnification was to be able to quickly determine the mean strains. This only required stitching 3 images together per deformation and performing the DIC analysis. The higher magnification results were used in conjunction with the microstructural data to elucidate information about its effects on the strain heterogeneity. The stress–strain curve with each of the deformation steps marked is given in Fig. 7a. The deformation steps in terms of the mean $\varepsilon_{yy}$ strain were as follows: 0.02, 0.30, 1.06, 1.22, 1.37, 1.59, 1.87, 1.96, 2.51, and 3.09 %. The three DIC $\varepsilon_{yy}$ strain fields, Fig. 7b–d, are the higher magnification results from the 1.22, 1.59, and 2.51 % steps respectively.

The increasing strains are obvious in Fig. 7 when taking into account the scales. The use of both DIC strain fields and microstructure data from EBSD provided insight into the main areas of strain concentration during the deformation.

To quantitatively find results, the strains were analyzed globally. Figure 8 presents these results. In Fig. 8a, a histogram depicts the changing strain values for four of the deformation steps. It is observed that there is a clear shift from a peak of concentrated values for Step 2 (mean $\varepsilon_{yy}$ strain of 0.32 %) to a broad extended distribution of strains in Step 9 (mean $\varepsilon_{yy}$ strain of 2.53 %). From this result and the heterogeneity shown in Fig. 7, it can be interpreted that some areas are deforming at a higher rate than others while certain areas are not deforming. A clearer picture of this is given in Fig. 8b which illustrates that the maximum strain is increasing at a quicker rate than the mean value. It is also noted that the minimum strain value is consistent throughout the entire experiment. The standard deviation of the $\varepsilon_{yy}$ strain field, plotted in Fig. 8c, quantitatively shows the increase of heterogeneity perceived from the other figures.

Since the EBSD data is rich with information about grain orientations and grain boundary types, it is possible to combine this with the DIC results to look at the activated slip systems. The method used can be found in [21]. For brevity since the focus of this paper is about abilities and the high temperature technique, only two slip systems (7 and 8) have been shown. The corresponding slip plane and slip direction

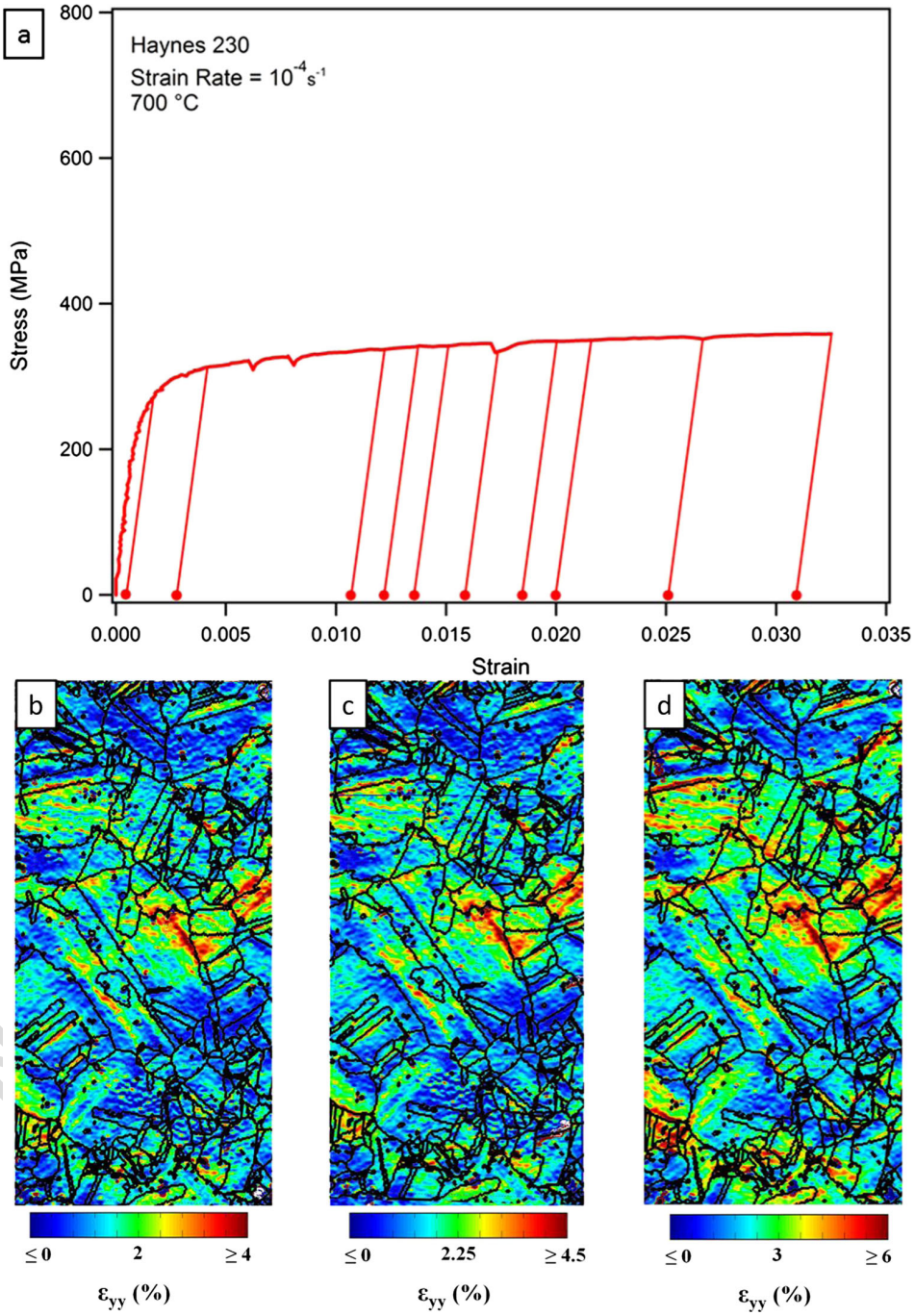


**Fig. 7** (**a**) The stress–strain response of Haynes 230 experimented at 700 °C with the 10 steps of deformation indicated when the experiment was halted to image for DIC. The $\varepsilon_{yy}$ strain field of the 1.05 mm by 0.525 mm area studied with the grain and twin boundaries overlaid at mean strains of (**a**) 1.22 %, (**b**) 1.59 %, and (**c**) 2.51 %. Note the scale bar changes for each strain field

for these systems are highlighted in Table 2. Figure 8 (system 7) and Fig. 9 (system 8) show the results from deformation step 6. The dark blue areas (0 % strain) indicate that that respective system has not been activated in the grain. The areas boxed and magnified show an annealing twin, a Σ3 boundary using the CSL notation, inside of a grain. The Schmid factors for the twin and grain are given in Table 2. Figure 8 clearly shows that slip is transmitted through the grain and twin boundaries, while in Fig. 9 the Σ3 twin boundary blocks the slip transmission. This is important for studying crack initiation as this can determine the creation of a grain cluster when slip is transmitted or an area of strain concentration in the case of blocking. Further global analysis of this can be performed, including the relationship between strain and residual Burgers vectors [21].

Another part of the microstructure that must be noted is the carbides that are present in this material. Two types of carbides have been identified in several studies of Haynes 230: $M_6C$

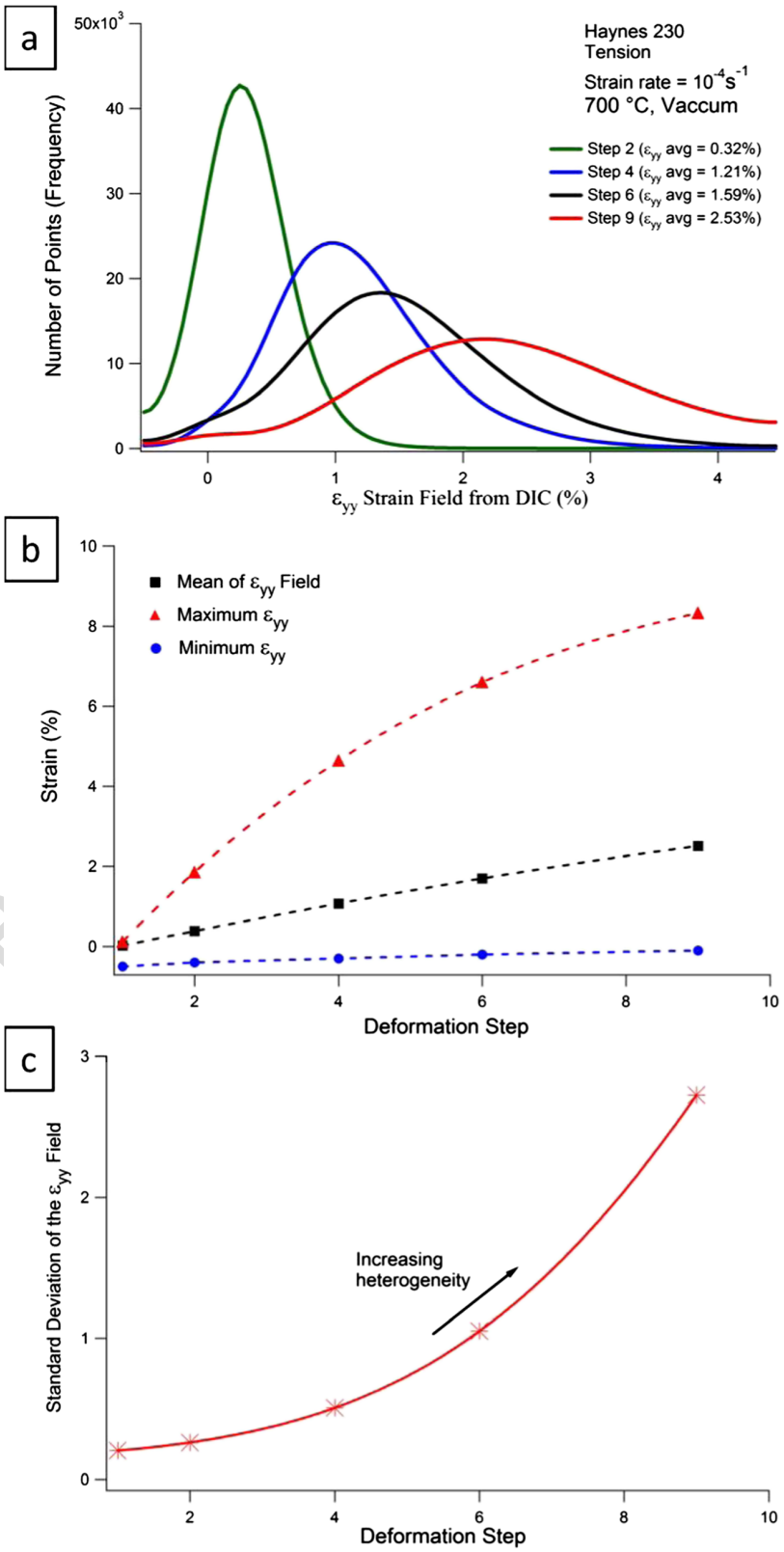


**Fig. 8** (**a**) Histogram of the strain values for four deformation steps showing the increasing strain values. (**b**) The trends of the minimum, maximum, and mean values of the $\varepsilon_{yy}$ strain field for each deformation step. (**c**) The standard deviation of the $\varepsilon_{yy}$ strain field showing an increasing heterogeneity in the strain field

**Table 2** Schmid factors for the 12 slip systems of the grain and twin shown in Fig. 9

| Slip system, $\alpha$ | Slip plane | Slip direction | Schmid factor (Twin) | Schmid factor (Grain) |
|---|---|---|---|---|
| System 1 | (111) | $[1\bar{0}]$ | 0.33 | 0.03 |
| System 2 | (111) | $[10\bar{1}]$ | 0.40 | 0.01 |
| System 3 | (111) | $[01\bar{1}]$ | 0.07 | 0.02 |
| System 4 | $(\bar{1}1)$ | [101] | 0.38 | 0.40 |
| System 5 | $(\bar{1}1)$ | $[01\bar{1}]$ | 0.09 | 0.46 |
| System 6 | $(\bar{1}1)$ | [110] | 0.47 | 0.07 |
| System 7 | $(1\bar{1})$ | $[\bar{0}1]$ | 0.37 | 0.27 |
| System 8 | $(1\bar{1})$ | [011] | 0.05 | 0.36 |
| System 9 | $(1\bar{1})$ | [110] | 0.33 | 0.09 |
| System 10 | $(11\bar{1})$ | $[1\bar{0}]$ | 0.46 | 0.19 |
| System 11 | $(11\bar{1})$ | [101] | 0.39 | 0.11 |
| System 12 | $(11\bar{1})$ | [011] | 0.07 | 0.08 |

and $M_{23}C_6$ [24, 25]. The M in the $M_6C$ carbide is assumed to be mostly the tungsten while the M in the $M_{23}C_6$ carbide is assumed to be chromium. The DIC analysis begins to show failed correlations after the third deformation step at the locations that EBSD revealed carbides. This indicates that the carbides are much more rigid than the rest of the material and play an important role in the deformation at high temperatures. A previous study of creep indicated that carbides at grain or twin boundaries in Haynes 230 are likely to pin the boundary and prevent sliding reducing creep strain, but eventually leading to a failure of the boundary [25]. This is a possible explanation for the large amount of strain concentrated at boundaries and the cracking observed in the 800 °C experiment. In order to glean all the information provided by this experiment, a full analysis of the grain boundary types with strain concentrations, active slip systems, and the impact on strain near carbides is required. This is outside the scope of this study.

## Conclusions

This study presented a new experimental methodology for studying materials at high temperatures with high resolution digital image correlation in conjunction with microstructure data. Previous limitations of the speckle pattern changing due to the conditions in an elevated temperature environment were overcome by using stable alumina particles for a speckle pattern and preventing oxidation by experimenting in vacuum. Using this technique, it is possible to study phenomena such as creep, creep-fatigue, and high temperature monotonic

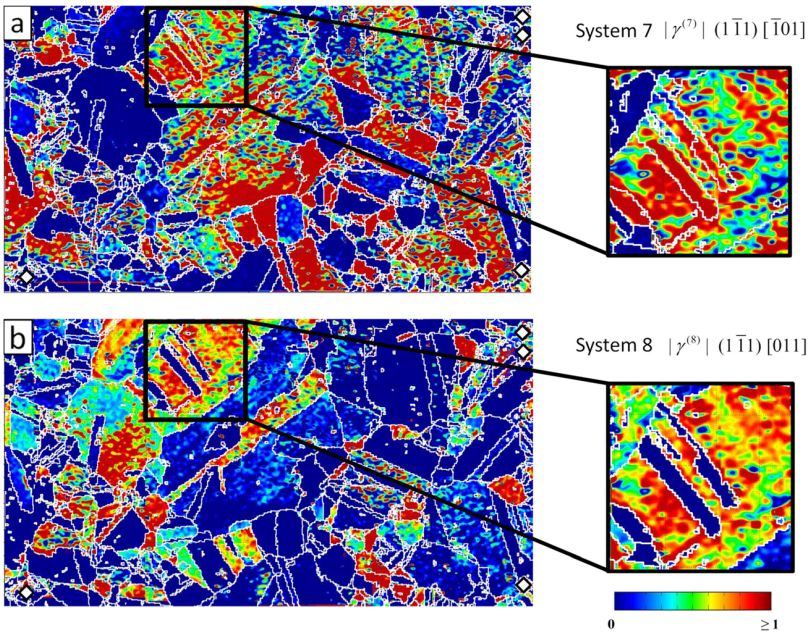


**Fig. 9** (**a**) Slip system 7 and (**b**) slip system 8 shear increments after deformation step 4. The dark blue areas are where the system has not been activated. (**a**) Slip transmission between a grain and twin is depicted in the magnified box. (**b**) Blockage of slip from the grain to the twin is shown in the magnified box. See Table 2 for the Schmid factor values

tension. DIC was performed on images that were stitched and an additional, alternative approach of correlating each individual image and then stitching the DIC results was used. Repeatability of this technique was proven by studying Haynes 230 under a tensile load at temperatures of 700 °C and 800 °C with multiple deformation steps. A method was developed to recover the focus of areas with out of plane displacement, seen after crack formation in the present study, in order to image the surface for DIC analysis. Strain heterogeneity was observed throughout along areas of slip activity, grain boundaries, and triple points with strains at these locations typically 2 % or greater than the mean strain of the region. An error analysis was performed and the errors observed were small compared to the measured strains. This study represents a substantial effort to advance the practicality of DIC for studying materials in a variety of environments with a high resolution in order to elucidate information about the microstructure's effects on strain heterogeneities commonly seen during loading.

**Acknowledgments** The research was supported by the US Department of Energy Nuclear Energy University Program (NEUP) under grant DOE-INL-00091210.

## References

1. Argon AS (2012) Strengthening mechanisms in crystal plasticity. Oxford University Press, Inc, New York
2. Wilkinson AJ, Meaden G, Dingley DJ (2006) High resolution mapping of strains and rotations using electron backscatter diffraction. Mater Sci Technol 22(11):1271
3. Wright SI, Nowell MM, Field DP (2011) A review of strain analysis using electron backscatter diffraction. Microsc Microanal 17(03): 316–329. doi:10.1017/S1431927611000055
4. Soula A, Renollet Y, Boivin D, Pouchou JL, Locq D, Caron P, Bréchet Y (2009) Analysis of high-temperature creep deformation in a polycrystalline nickel-base superalloy. Mater Sci Eng A 510–511:301
5. Thibault K, Locq D, Caron P, Boivin D, Renollet Y, Bréchet Y (2013) Influence of microstructure on local intra- and intergranular deformations during creep of a nickel-based superalloy at 700 °C. Mater Sci Eng A 588:14
6. Badulescu C, Grediac M, Haddadi H, Mathias JD, Balandraud X, Tran HS (2011) Applying the grid method and infrared thermography to investigate plastic deformation in aluminium multicrystal. Mech Mater 43(1):36–53. doi:10.1016/j.mechmat.2010.11.001
7. Delaire F, Raphanel JL, Rey C (2000) Plastic heterogeneities of a copper multicrystal deformed in uniaxial tension: experimental study and finite element simulations. Acta Mater 48(5):1075–1087
8. Héripré E, Dexet M, Crépin J, Gélébart L, Roos A, Bornert M, Caldemaison D (2007) Coupling between experimental measurements and polycrystal finite element calculations for micromechanical study of metallic materials. Int J Plast 23(9):1512–1539
9. Rastogi P, Surrel Y (2000) Fringe Analysis. In: Photomechanics, vol 77. Topics in Applied Physics. Springer Berlin Heidelberg, pp 55–102
10. Sutton M, Orteu J-J, Schreier H (2009) Image Correlation for Shape Motion and Deformation Measurements: Basic Concepts, Theory and Applications. Spring Media,
11. Pataky GJ, Sehitoglu H, Maier HJ (2013) High temperature fatigue crack growth of Haynes 230. Mater Charact 75:69
12. Sangid MD, Pataky GJ, Sehitoglu H, Rateick RG, Niendorf T, Maier HJ (2011) Superior fatigue crack growth resistance, irreversibility, and fatigue crack growth microstructure relationship of nanocrystalline alloys. Acta Mater 59(19):7340
13. Lyons JS, Liu J, Sutton MA (1996) High-temperature deformation measurements using digital-image correlation. Exp Mech 36(1):64–70
14. Merzouki T, Collard C, Bourgeois N, Ben Zineb T, Meraghni F (2010) Coupling between measured kinematic fields and multicrystal SMA finite element calculations. Mech Mater 42(1):72–95
15. Zhao Z, Ramesh M, Raabe D, Cuitino AM, Radovitzky R (2008) Investigation of three-dimensional aspects of grain-scale plastic surface deformation of an aluminum oligocrystal. Int J Plast 24(12):2278
16. Sutton MA, Li N, Joy DC, Reynolds AP, Li X (2007) Scanning electron microscopy for quantitative small and large deformation measurements part I: SEM imaging at magnifications from 200 to 10,000. Exp Mech 47(6):775–787
17. Carroll J, Abuzaid W, Lambros J, Sehitoglu H (2010) An experimental methodology to relate local strain to microstructural texture. Rev Sci Instrum 81(8):083703. doi:10.1063/1.3474902
18. Jonnalagadda KN, Chasiotis I, Yagnamurthy S, Lambros J, Pulskamp J, Polcawich R, Dubey M (2010) Experimental investigation of strain rate dependence of nanocrystalline Pt films. Exp Mech 50(1):25–35
19. Pan B, Wu D, Wang Z, Y. X (2011) High-temperature digital image correlation method for full-field deformation measurement at 1200 °C. Meas Sci Technol. 22 (1). doi:10.1088/0957-0233/22/1/015701
20. Preibisch S, Saalfeld S, Tomancak P (2009) Globally optimal stitching of tiled 3D microscopic image acquisitions. Bioinformatics 25(11):1463–1465. doi:10.1093/bioinformatics/btp184
21. Abuzaid WZ, Sangid MD, Carroll JD, Sehitoglu H, Lambros J (2012) Slip transfer and plastic strain accumulation across grain boundaries in Hastelloy X. J Mech Phys Solids 60(6):1201–1220. doi:10.1016/j.jmps.2012.02.001
22. Carroll JD, Clark BG, Buchheit TE, Boyce BL, Weinberger CR (2013) An experimental statistical analysis of stress projection factors in BCC tantalum. Mater Sci Eng A 581:108
23. Swaminathan B, Lambros J, Sehitoglu H (2013) Digital image correlation study of mechanical response of nickel superalloy hastelloy X under thermal and mechanical cycling: uniaxial and biaxial stress states. J Strain Anal Eng Des. doi:10.1177/0309324713503959
24. Jiang L, Hu R, Kou H, Li J, Bai G, Fu H (2012) The effect of M23C6 carbides on the formation of grain boundary serrations in a wrought Ni-based superalloy. Mater Sci Eng A 536:37
25. Pataky GJ, Sehitoglu H, Maier HJ (2013) Creep deformation and mechanisms in Haynes 230 at 800 °C and 900 °C. J Nucl Mater 443(1–3):484